Corrosion Science 114 (2017) 72–78

Contents lists available at ScienceDirect

Corrosion Science

journal homepage: www.elsevier.com/locate/corsci

Non-uniform film growth and micro/macro-galvanic corrosion of copper in aqueous sulphide solutions containing chloride

J. Chen, Z. Qin, T. Martino, D.W. Shoesmith*

Department of Chemistry and Surface Science Western, Western University, London, Ontario N6A 5B7, Canada

ARTICLE INFO

Article history:
Received 20 June 2016
Received in revised form 21 October 2016
Accepted 22 October 2016
Available online 23 October 2016

Keywords:
A. Copper
B. SEM
C. Interfaces

ABSTRACT

The corrosion of copper in aqueous sulphide environments is rapid and can occur under transport limited conditions. At sufficiently high sulphide flux, microgalvanic corrosion can be supported between areas of the surface covered by compact sulphide deposits and other areas covered only by a porous deposit. This leads to excessive crystal growth at the cathodes (compact film) and localized corrosion damage at the anodes (porous film). The transport of Cu(I) between the two areas, required to sustain this process, appears to occur predominantly by the solution transport of Cu-sulphide complex or clusters.

1. Introduction

Precipitation and crystal growth involve a phase transition from a high energy solvated state to a lower energy location in the crystalline phase [1] and can be influenced by features such as the properties of the solvent, the presence of impurities and the substrate grain orientation and, for corrosion processes, the cathodic current density [1–11]. These influences can lead, for corroding systems, to a non-uniform growth of the corrosion film which could influence the distribution of corrosion damage.

In aqueous solutions, sulphide destabilizes Cu at very negative corrosion potentials, leading to its corrosion and the deposition of films on the Cu surface. Previously, we have shown [12–17] that corrosion is rapid, leading to the deposition of chalcocite (Cu_2S), identified by energy dispersive X-ray spectroscopy (EDS), X-ray photoelectron spectroscopy (XPS) and X-ray diffraction (XRD). This layer is formed at the Cu_2S/electrolyte interface with the total consumption of sulphide [12]. Under stagnant and controlled convective conditions the morphology of film growth was markedly influenced by transport processes. In a stagnant solution, corrosion was controlled by solution transport, and a non-protective film composed of crystals with a wide distribution of sizes was formed. When the transport process was convectively accelerated, a more coherent and partially protective film with a narrow distribution of crystal sizes was formed. This sensitivity to transport, and the wide distribution in the size of corrosion product crystals when transport is uncontrolled (i.e., under stagnant conditions), suggests local variations in corrosion rate. This raises the spectre that corrosion damage to the Cu substrate will be non-uniform. If this is indeed the case then the commonly adopted specification of a corrosion allowance for nuclear waste containers in lifetime prediction models in Sweden, Finland and Canada [18–20] should be re-examined.

In this paper we describe a series of experiments to determine the details of the corrosion process with a primary emphasis on understanding how the wide distribution in crystal growth rates develops and its role in determining the distribution of damage across the corroded surface. The implications for the corrosion of nuclear waste containers are also addressed. In experiment (i) a Cu specimen was immersed in the solution for 1691 h under natural corrosion conditions. In experiment (ii) half the surface of a Cu specimen was sealed with wax while the other half was exposed to the solution. This partially wax-sealed specimen was then immersed in the solution for 1211 h before the wax was removed and the specimen re-immersed in the same solution for a further 480 h for a total immersion time of 1691 h. In experiment (iii) a Cu specimen was pre-corroded in the solution for 1211 h and then re-immersed galvanically connected to an uncorroded Cu specimen for a further 480 h for a total immersion time of 1691 h.

2. Materials and methods

Experiments were conducted using P-doped (30–100 mg/kg), O-free copper (Cu-OF) provided by the Swedish Nuclear Fuel and Waste Management Co. (SKB), Stockholm. Cu disk working electrodes (1×10^{-2} m in diameter) were cut from plate material. The

* Corresponding author.
E-mail address: dwshoesm@uwo.ca (D.W. Shoesmith).

http://dx.doi.org/10.1016/j.corsci.2016.10.024
0010-938X/

disks were connected to a stainless steel shaft and painted with a non-conductive lacquer to prevent contact of the Cu/steel junction with the solution. The electrodes were then heated (60 °C for 12 h) to promote adhesion of the paint. The exposed flat surface was ground successively with 240, 600, 800, 1000, 1200 grade SiC paper, then polished to a mirror finish using 1 μm, 0.3 μm, and, finally, 0.05 μm Al_2O_3 suspensions. Prior to experiments, electrodes were washed with Type I water (resistivity = 18.2 MΩ·cm (obtained from a Thermo Scientific Barnstead Nanopure 7143 ultrapure water system)), ultrasonically cleaned using methanol (reagent grade), washed with Type I water, and dried using ultra pure Ar.

To ensure anoxic conditions, experiments were performed in an Ar-purged anaerobic chamber (Canadian Vacuum Systems Ltd.), maintained at a positive pressure (2–4 mbar) by an MBraun glove box control system. The oxygen concentration in the chamber was analyzed with an MBraun oxygen probe with a detection limit of 1.4 mg/m^3. The anaerobic chamber was maintained at a total oxygen concentration ≤4.2 mg/m^3, which includes the oxygen in both air and vapor. The actual oxygen content of the solution should be less than this value. Even though there is a trace amount of oxygen present, copper sulphide is more stable in sulphide solution than copper oxide based on thermodynamic data (The standard free energy of reaction, $\Delta G^\circ = -101.46$ kJ/mol, for the conversion from Cu_2O to Cu_2S in sulphide solutions at 298 K [21]: Cu_2O (s) + HS^- (aq) → Cu_2S (s) + OH^- (aq)) and available literature [22–25].

The 0.1 mol/L NaCl + x mol/L Na_2S solution (x = 5×10^{-5}, 5×10^{-4} and 1×10^{-3} mol/L) was prepared with Type I water, reagent-grade sodium sulphide ($Na_2S{\cdot}9H_2O$, 98.0% assay) and sodium chloride (NaCl, 99.0% assay), to simulate the saline groundwater conditions anticipated in a waste repository.

Electrodes were immersed in the sulphide solutions under natural corrosion conditions (at the corrosion potential, E_{CORR}) for various exposure periods. A standard three-electrode cell with a Pt plate counter electrode and a saturated calomel reference electrode (SCE) was used. Prior to each experiment, electrodes were cathodically cleaned at −1.6 V/SCE for 2 min and then at −1.15 V/SCE for 2 min.

Since exposure periods were long, the [SH^-] was monitored weekly by measuring the pH as described previously [12] and SH^- added to readjust the [SH^-] to its original value. Experiments were performed at 25 ± 2 °C. Corrosion potentials (E_{CORR}) were measured using a Solarton 1287 electrochemical interface and, in galvanically-coupled experiments, the current density was measured using a Keithley 6514 electrometer.

Electrodes removed from solution for surface analyses were rinsed with Type I water for 10 min and dried with cold Ar gas. Analyses were then performed after a minimum period of interim storage (<30 min). The surface and cross-sectional morphologies of corroded specimens were observed using a Leo 1540 scanning electron microscope (SEM) equipped with a focused ion beam (FIB) (Zeiss Nano Technology Systems Division, Germany). The composition of films was qualitatively analyzed by energy dispersive X-ray spectroscopy (EDS) using a Leo 1540 FIB/SEM microscope (the oxygen detection limit is 1 at.%). The Cu content of solutions was analyzed using inductively coupled plasma atomic emission spectroscopy (ICP-AES).

3. Results and discussion

3.1. The phenomenon of excessive crystal growth

Fig. 1 shows the Cu_2S film formed on Cu after 1691 h of immersion in a 0.1 mol/L NaCl + 5×10^{-4} mol/L Na_2S solution (experiment (i)). Most of the surface is covered with a relatively uniform deposit while some areas have experienced excessive crystal growth as

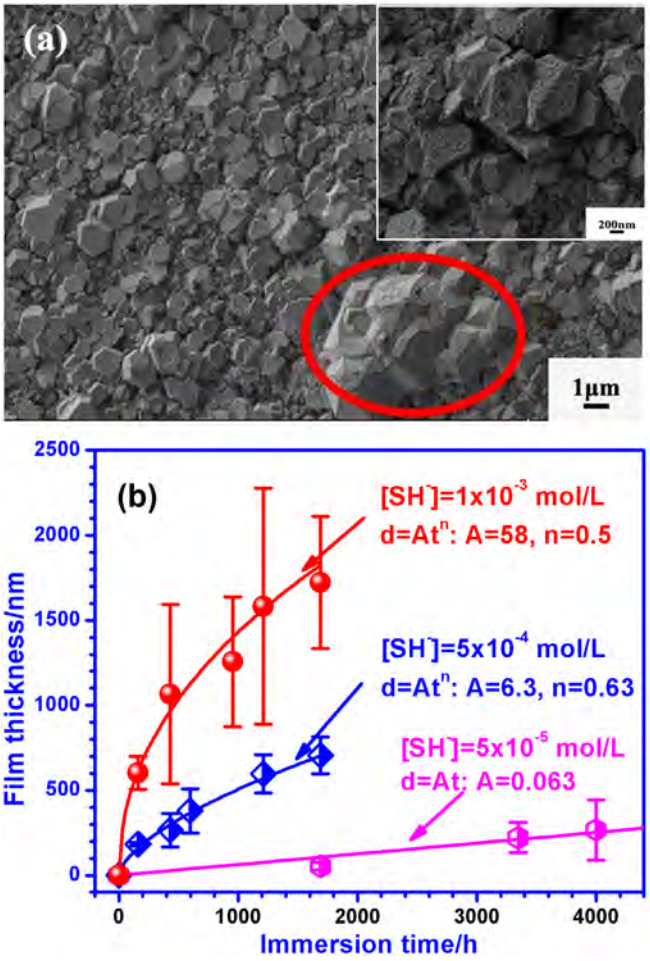

Fig 1. (a) An example of excessive crystal growth on Cu (indicated within the red oval) with an insert showing the surface at high magnification after 1691 h immersion 0.1 mol/L NaCl + 5×10^{-4} mol/L Na_2S solution; and (b) film thickness as a function of immersion time for sulphide films grown in 0.1 mol/L NaCl solutions containing various [SH^-] [12,13,15]. The growth rate laws are indicated for each [SH^-]. All of these experiments were performed under natural corrosion conditions. The film growth kinetics in Fig. 1b is cited from Ref. [15]. The linear least squares/linear fit to the experiment data is given as solid line in Fig. 1b, with a fitting dependency of >0.98. The fitting detail have been described in Ref. [12]. (For interpretation of the references to colour in this figure legend, the reader is referred to the web version of this article.)

indicated within the oval, Fig. 1(a). Fig. 1(b) shows the film growth kinetics in 0.1 mol/L NaCl solution containing various [SH^-], based on many thickness (d) measurements at various locations in FIB (focused ion beam)-cut cross sections. As shown in Fig. 1a, the film grew non-uniformly leading to the variations in thickness with location. The error bars in Fig. 1b show the standard deviations calculated from this series of measurements. The plotted lines show the linear least squares fits to the data used to obtain the growth laws.

When [SH^-] is low (i.e., 5×10^{-5} mol/L Na_2S), film growth kinetics are linear and, as shown elsewhere [13], the film develops a cellular structure. Impedance measurements showed [13] the rate of interfacial reaction is larger than the diffusive flux of SH^- to the corroding surface, and Cu_2S growth is controlled primarily by SH^- diffusion in solution consistent with the linear growth of a non-protective film. However, when [SH^-] is high (1×10^{-3} mol/L), the film deposits with a well defined crystal structure, and the growth kinetics are parabolic indicating the diffusive flux is greater than the interfacial reaction rate leading to film growth controlled by Cu^+ diffusion in the now protective film. In addition, as [SH^-] increases,

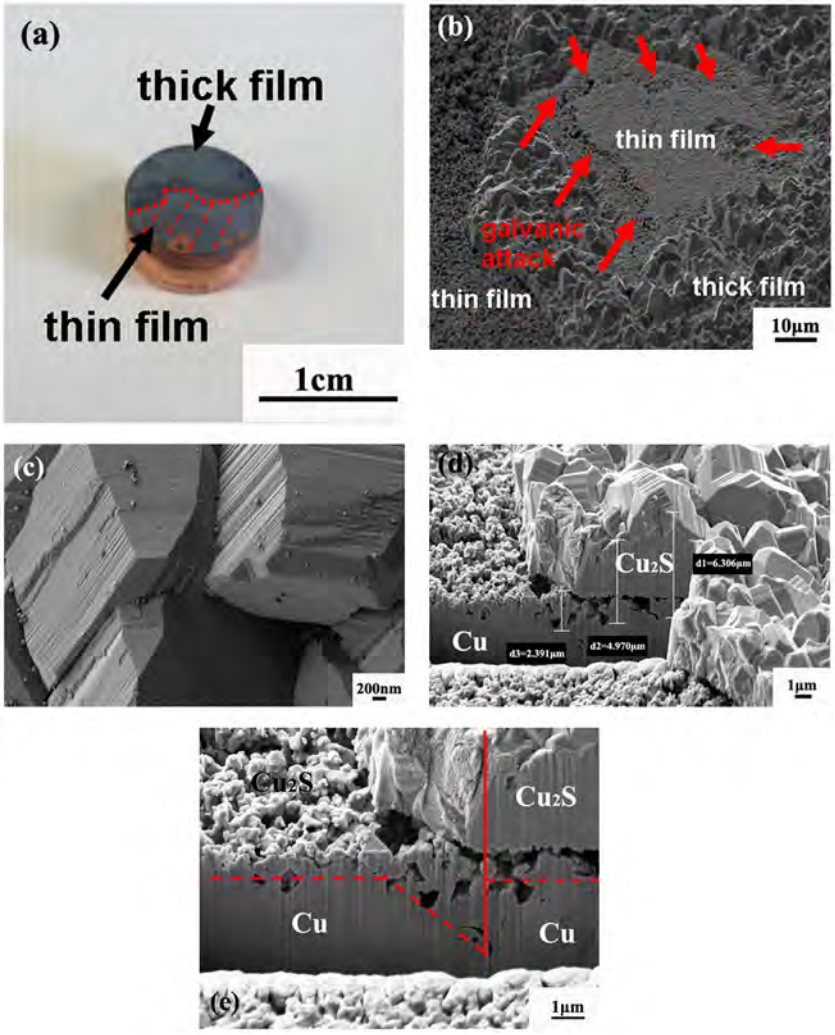

Fig. 2. (a) Photograph of the surface of the Cu specimen from experiment (ii) after 1691 h exposure in 0.1 mol/L NaCl + 5×10^{-4} mol/L Na_2S solution: the area marked "thick film" was exposed to solution for the whole exposure period, and the area marked "thin film" and defined by the dashed red lines was wax-covered for 1211 h and then exposed for the final 480 h. The boundary between the two areas is indicated by the dotted red line; (b) SEM micrograph showing a location at the interface between "thick film"/"thin film" regions in Fig. 2(a) where both regions are visible; (c) SEM micrograph showing the crystalline film formed on the thick film area; (d) and (e), FIB cut cross sections showing the Cu/Cu_2S interface at the junction of the thick and thin film regions. In (e) the vertical red line indicates the junction between the thick and thin film regions and the dashed red line the Cu/Cu_2S interface. (For interpretation of the references to colour in this figure legend, the reader is referred to the web version of this article.)

the distribution in film thickness (indicated by the standard deviations) increases markedly, demonstrating that excessive crystal growth becomes more pronounced at higher [SH^-].

3.2. Natural corrosion

After the specimen was corroded for 1691 h (experiment (i)), a compact crystalline film was formed. These crystals were generally covered with a fine particulate deposit with individual particles experiencing excessive growth (inset, Fig. 1(a)). A FIB cut cross section (not included) showed that the film was a single compact layer with an average thickness of ~700 nm. On completion of the experiment after 1691 h, the analyzed Cu content of the solution was below the detection limit (<4 mg m^{-3}).

3.3. Evidence for microgalvanic corrosion

Fig. 2 shows the surface of the partially wax-sealed Cu specimen after exposure for the total immersion period, experiment (ii). Two distinct areas were observed, Fig. 2(a). The originally exposed area was covered with a thick Cu_2S film ("thick film") while on the initially wax-covered area, a thin Cu_2S deposit ("thin film") was observed. The well-defined crystals formed on the "thick film" area were similar to those formed on the naturally-corroded Cu specimen (experiment (i)), Fig. 1(a), while the film formed on the "thin film" area over the final 480 h of the experiment, was porous, Fig. 2(b). The red arrows indicate significant galvanic corrosion on the exposed "thin film" region.

While similar to the film formed in experiment (i) the crystals in the thick film region in experiment (ii) were remarkably larger (~2–4 μm), Fig. 2(c). The film in this region was ~4–6 μm thick, Fig. 2(d), 7 to 8 times thicker than the film formed on the naturally-corroded specimen (experiment (i)) after the same exposure time. Inspection of the junction between the thick/thin film regions shows this location was the most extensively corrosion damaged, Fig. 2(e), especially in the direct vicinity of the junction. This is a characteristic feature of micro-galvanic corrosion with the larger crystals in the thick film covered area acting as cathodes in support of the anodes located in the poorly protective thin film region. This distribution of corrosion damaged anodes accompa-

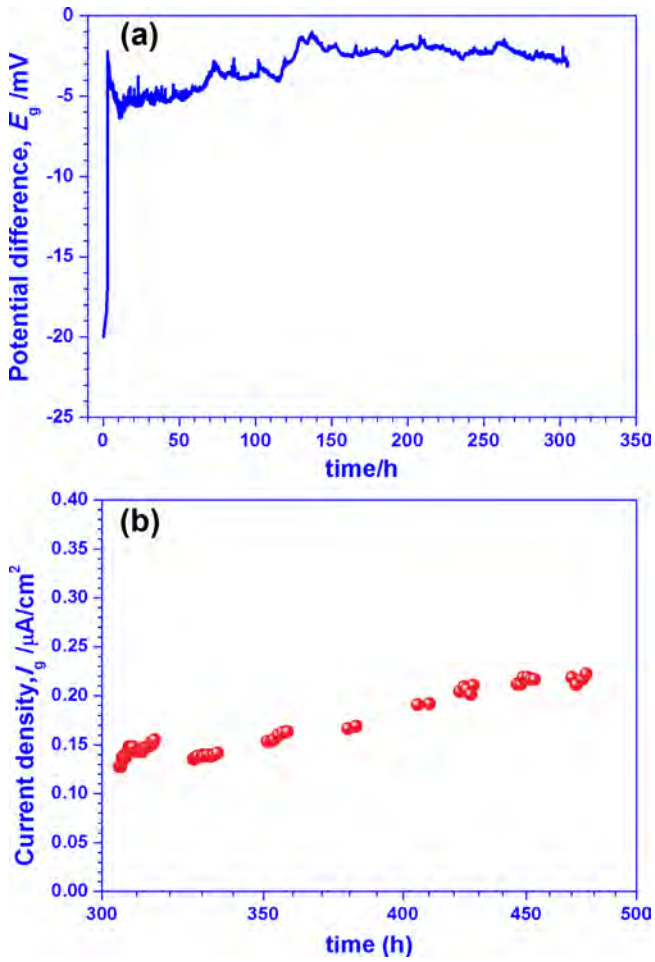

Fig. 3. (a) Potential difference between the pre-corroded specimen (serving as reference electrode) and the uncorroded galvanically coupled specimens; and (b) the galvanic current density flowing between the pre-corroded specimen acting as the coupled cathode and the uncorroded specimen acting as the coupled anode. Note, the potential difference and galvanic current density were measured over consecutive periods.

nied by the deposition of corrosion product on adjacent cathode surfaces has been commonly observed for galvanically-corroding systems [26–37]. A more extensive study on the influence of the relative cathode and anode areas, their separation and the influence of temperature and groundwater composition is underway.

3.4. Evidence for macrogalvanic corrosion

While experiment (ii) suggests that microgalvanically-coupled corrosion occurred it offers little information on the details of the process, in particular the strength and activity of the galvanic reaction. To investigate these features a pre-corroded specimen (for 1211 h making it equivalent to the specimen from experiment (ii)) was galvanically coupled to an uncorroded specimen, experiment (iii). In this last experiment (iii) one specimen was pre-corroded in 0.1 mol/L NaCl + 5×10^{-4} mol/L Na_2S solution for 1211 h at E_{CORR}. A second specimen with the same surface area (0.785 cm^2) was then immersed in the same solution at a distance of 5 cm from the pre-corroded specimen. The pre-corroded specimen was selected as the reference electrode and the uncorroded specimen as the working electrode when recording the potential difference (E_g) between them, Fig. 3(a). After measuring the potential difference for 300 h, the galvanic current (I_g) passing between the two specimens was measured till the total immersion time of the pre-corroded specimen was 1691 h, Fig. 3b. The E_g was ~2 to 6 mV and I_g was up to ~0.1 μA/cm^2, confirming the establishment of a galvanic couple, the pre-corroded specimen acting as the net cathode and the uncorroded specimen as the net anode.

Fig. 4 shows the surface and cross-sectional morphologies of the net anode and the net cathode after their total immersion times (480 h and 1691 h, respectively). Excessive crystal growth (indicated within the oval in Fig. 4(a)) was observed on the initially uncorroded electrode (the net anode), indicating the occurrence of micro-galvanic coupling, and the cross section, Fig. 4(b) and (c), clearly shows a thick crystalline film over a relatively undamaged substrate adjacent to a more deeply corroded substrate covered only with a porous thinner layer. That this microgalvanic corrosion was accompanied by significant macrogalvanic corrosion over the final 480 h exposure period was confirmed by comparison of the crystalline deposits formed in experiments (iii) and (i), which shows the crystals on the net cathode (in experiment (iii)) were larger and the deposited film 3 to 6 times thicker (~2–4 μm) than that formed on the naturally-corroded surface (experiment (i)).

These observations show that the macrogalvanic corrosion due to the coupling of the two electrodes accompanies the microgalvanic corrosion occurring simultaneously on both electrodes. The steady increase in I_g with time could reflect the increasing area of the net cathode as the large crystals grow by deposition of Cu transported from the net anode, and suggests the cathodic reaction is rate determining. Analysis of the solution on completion of the experiment detected 11 mg m^{-3} of Cu confirming the presence of a solution transport process.

3.5. Model for microgalvanic corrosion leading to excessive crystal growth

Anion adsorption on Cu is well documented [38–46], and sulphide adsorption to form the chemisorbed species, $Cu(SH)_{ads}$, has been shown to be a precursor to sulphide film formation, leading to a negative shift in corrosion potential (E_{CORR}) of Cu [12–17],

$$Cu + SH^- \rightarrow Cu(SH)_{ads} + e^- \quad (1)$$

with SH^- being the dominant species (in solution) since the pK_a (pK_a = −log K_a, K_a is the acid dissociation constant) is large and in the range 11.96 to 18 [47–49].

This chemisorbed species then reacts with Cu and SH^- leading to the deposition of Cu_2S on the Cu surface (Fig. 1) [12–17]. By analogy to geologic environments [50,51], this process would proceed via the formation of complexes such as $CuSH^0$, $Cu(SH)_2^-$ and $Cu_2S(SH)_2^{2-}$ with $Cu(SH)_2^-$ being dominant [51] in an aqueous solution with high sulphide content (i.e. 0.1 mol/L NaCl + 5×10^{-4} mol/L Na_2S solution):

$$Cu(SH)_{ads} + SH^- \rightarrow Cu(SH)_2^- \quad (2.1)$$

$$Cu + Cu(SH)_2^- \rightarrow Cu_2S + H_2S + e^- \quad (2.2)$$

$$\text{Overallreaction}: Cu + Cu(SH)_{ads} + SH^- \rightarrow Cu_2S + H_2S + e^- \quad (2)$$

Subsequently, the film would then thicken either via a parabolic growth law controlled by Cu^+ diffusion through the film (when the availability of SH^- is not transport limited in the solution) or via a linear growth law controlled by SH^- diffusion in the solution.

The corrosion of Cu in sulphide solutions is rapid since the corrosion potential, E_{CORR}, is close to the equilibrium potential for the Cu/Cu_2S reaction [12], i.e., the reaction requires only a small overpotential. Additionally, E_{CORR} increases with an increase in immersion time until steady state is reached [12], indicating that film formation changes the anodic dissolution kinetics of Cu even though the sulphide film is electrically conductive [12]. Consequently, the difference in film thickness leads to a potential

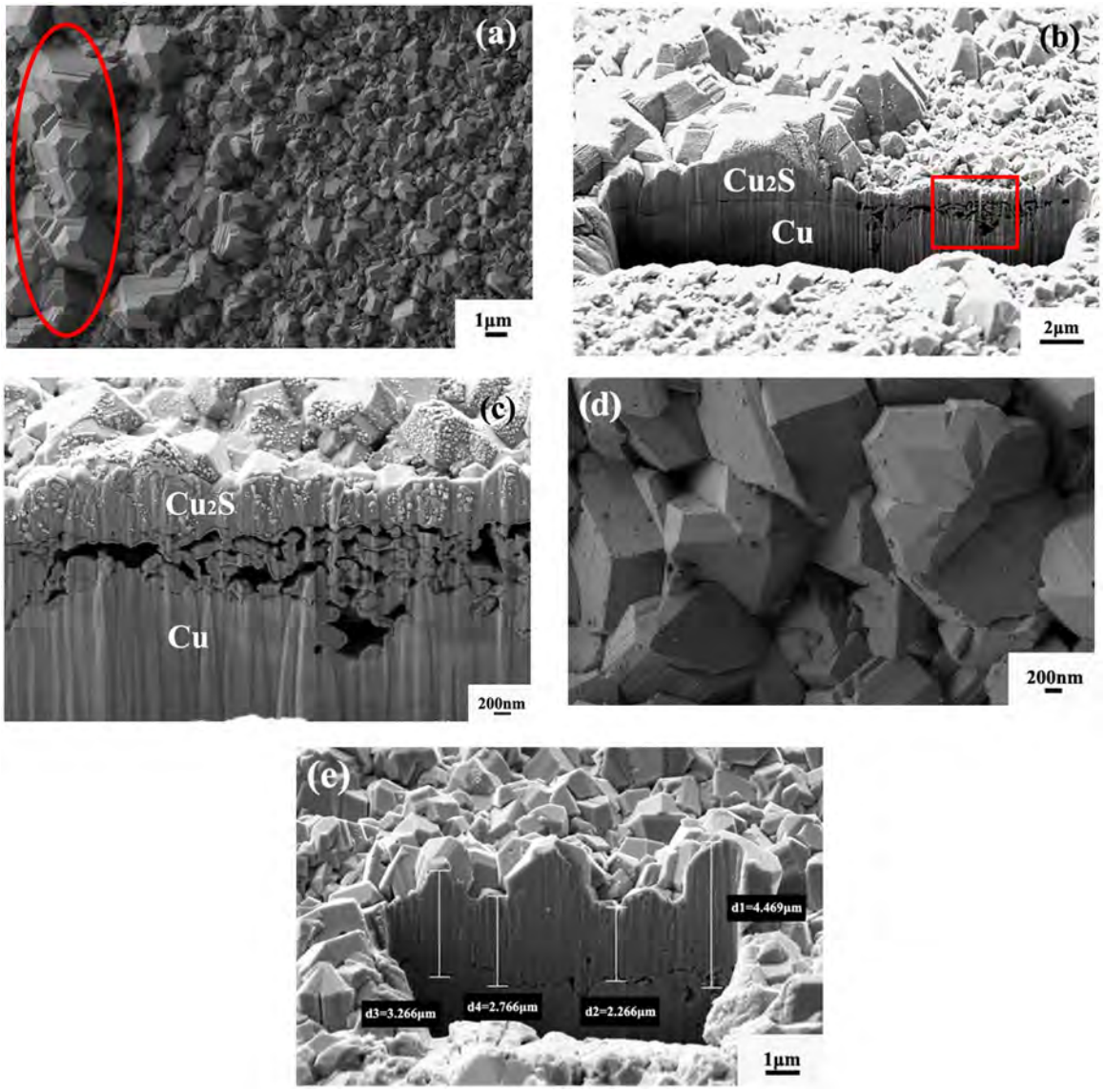

Fig. 4. (a) SEM micrograph of the surface of the net anode in experiment (iii) after 480 h immersion in 0.1 mol/L NaCl + 5 × 10^{-4} mol/L Na_2S solution; (b) and (c) FIB cut cross sections of a microgalvanically corroded location (Fig. 4(c)), a high magnification of area within the rectangle in Fig. 4(b)), (d) SEM micrograph of the surface of the net cathode in experiment (iii); and (e) FIB cut cross section of the net cathode. The markers indicate the film thickness.

difference between larger crystals in thicker films and smaller crystals in thinner films (experiments (ii) and (iii)). This potential difference accelerates the anodic dissolution of the net anode, which leads to $Cu(SH)_2^-$ enrichment and sulphide depletion at this region. When this situation prevails, the interfacial reaction rate will be faster than the sulphide diffusive flux, leading to the formation of porous film on the net anode [17] (Figs. Fig. 2(b) and Fig. 4(b)). In the pores where SH^- is significantly depleted, it is possible that the formation of soluble chloride complexes occurs via Reaction (3):

$$Cu(SH)_{ads} + 2Cl^- \rightarrow CuCl_2^- + SH^- \quad (3)$$

When transported out of the void space at the corroding anode such complexes would encounter an [SH^-] close to the bulk solution value at the outer film/solution interface and convert to $Cu(SH)_2^-$ which is considerably more stable in sulphide solutions [51],

$$CuCl_2^- + 2SH^- \rightarrow Cu(SH)_2^- + 2Cl^- \quad (4)$$

The pre-corrosion period (experiment (ii)), with ~50% of the electrode covered creates separated anodes and cathodes, subsequently exposed together over the final 480 h stage of the experiment, with the pre-corroded area expected to function as the cathode and the originally wax-covered area as the anode. If not micro-galvanically coupled in this manner, the originally wax-covered (uncorroded) area would corrode rapidly, leading to the accumulation of a relatively uniform Cu_2S deposit via a parabolic growth law (Fig. 1(b)), and the pre-corroded area, with a partially protective deposit, would corrode more slowly. However, by contrast, only a thin porous Cu_2S deposit was formed in the uncorroded area while the crystals continued to grow in the pre-corroded area. The enhanced corrosion damage observed at the junction between the two areas confirms that galvanic corrosion occurred.

Fig. 5 shows a schematic illustration of the microgalvanic process occurring in experiment (ii). Anodic polarization of the initially wax-covered area increased the interfacial reaction rate (Reaction (1)) leading to the formation of $Cu(SH)_2^-$ (Reaction (2.1)) and the depletion of sulphide in this region, with the interfacial reaction rate faster than the diffusive sulphide flux. This favored the

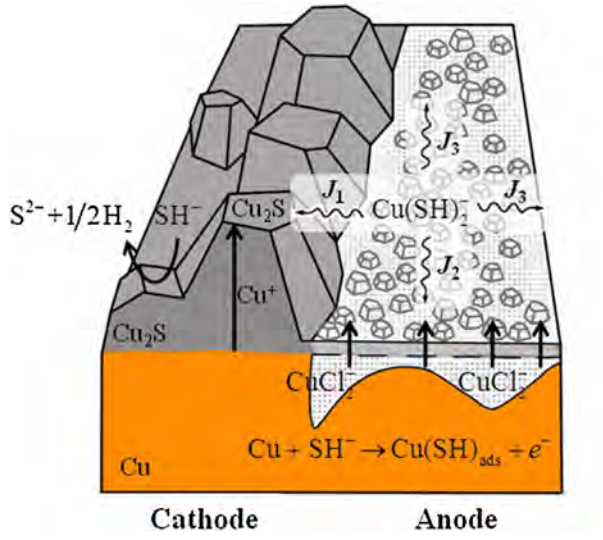

Fig. 5. Schematic of micro-galvanic corrosion process on the Cu electrode in 0.1 mol/L NaCl + 5×10^{-4} mol/L Na_2S solution, in which J_1 represents the $Cu(SH)_2^-$ flux towards the cathode, J_2 the $Cu(SH)_2^-$ flux towards the pore at the anode, and J_3 the $Cu(SH)_2^-$ flux towards other regions. J_1 is larger than J_2 and J_3 as a consequence of the $Cu(SH)_2^-$ concentration gradient and $Cu(SH)_2^-$ migration.

formation of a porous film at this location [17] whose growth was controlled by the transport of SH^- to the corroding surface [13]. Since the effective diffusion coefficient of SH^- in the pores in the film was much lower than that in the bulk solution [13], high-chloride/low-sulphide conditions were established within these pores, making Reaction (3) more favorable. This would lead to higher $CuCl_2^-$ concentration in the pores compared to the bulk solution, with the concentration gradient prompting the Cu transport through the pores. On encountering the bulk solution, $CuCl_2^-$ would convert to $Cu(SH)_2^-$ via Reaction (4). This enhanced $Cu(SH)_2^-$ concentration would then support Cu transport in the bulk solution.

The key features controlling the flux of $Cu(SH)_2^-$ are its diffusion coefficient, the concentration gradient and ionic migration. The presence of a local transport flux created by crystal growth at the cathodic sites [6], the $Cu(SH)_2^-$ concentration gradient, and $Cu(SH)_2^-$ migration due to potential difference between anode and cathode, establish a significantly larger $Cu(SH)_2^-$ flux towards the cathodic region (J_1) than towards other regions (J_2/J_3). This maintained Cu_2S crystal growth at the cathode and inflicted more extensive corrosion damage at the anode, Fig. 5. The flux of $Cu(SH)_2^-$ to the anode would be minimal as a consequence of its lower effective diffusion coefficient in the pores compared to that in bulk solution [13]. For this reason, the pores at the anode remained open.

The occurrence of macrogalvanic coupling in experiment (iii), can only be explained by a solution-based transport route, and the detection of analyzable amounts of Cu in the solution confirmed that one was available. Thermodynamic calculations suggest that $Cu(SH)_2^-$ is the dominant Cu(I)-sulphide complex present in 0.1 mol/L NaCl + 5×10^{-4} mol/L Na_2S solution [51]. As in experiment (ii), the $Cu(SH)_2^-$ concentration gradient and the potential difference between the cathode and anode would provide the driving force for transport of Cu from the net anode to the net cathode. This longer range transport through solution would make the Cu_2S deposit at the net cathode in experiment (iii) thinner and that at the net anode in experiment (iii) thicker (Figs. 2 and 4) than those in experiment (ii).

In natural environments, precipitation of metal cations can involve the initial formation of a metastable phase with a solubility >100 times the thermodynamically calculated values [52], and significant transport of metal sulphide species is known to occur in low [SH^-] (10^{-4} to 10^{-2} mol/kg) environments [53–55]. Based on EXAFS evidence, which suggests Cu-Cu nearest neighbor interactions [53], it has been claimed that Cu(I)-sulphide clusters and possibly nanoparticles [52] may account for such transport. These claims are supported by Fourier transform mass spectrometry studies which identified Cu and other metal cations as present in both laboratory and natural waters as Cu clusters or particles at concentrations up to ~600 nmol/L and 0.1 to 0.2 μm in size. Their presence was shown to sequester >90% of the SH^- in natural environments. Their formation would provide an alternative or accompanying transport pathway in experiments (ii) and (iii).

Our observation that micro-galvanic coupling was more marked at higher [SH^-] is also consistent with solubility and complexation constant measurements and indicates that this corrosion process would not be expected on Cu waste containers emplaced in a Swedish waste repository. While [SH^-] in the range 10^{-7} to 10^{-4} mol/L are expected, the fast reaction of Cu with SH^- would lead to the rapid depletion of SH^- at the container surface and in the compacted clay surrounding the container [20]. At the depressed surface [SH^-] Cu_2S film growth would be expected to be linear leading to porous films when micro-galvanic coupling would not be expected. Under these conditions the corrosion front on a container would be expected to be quite uniform and not subject to the local penetrations that would be a consequence of microgalvanic corrosion.

Two additional features of this study are relevant to the corrosion of copper waste containers. Our previously published electrochemical studies [12] indicated that formation of the Cu_2S corrosion product was 100% efficient; i.e., all the SH^- contacting the corroding surface was sequestered. This claim is supported by the environmental evidence that the formation of Cu sulphide species will efficiently sequester SH^- either as a corrosion product film or an environmentally transportable cluster/nanoparticle [51]. This study also confirms that the cathodic reaction leading to H_2 formation occurs at the Cu_2S/electrolyte interface on the conducting film. Whether or not this reaction can shift partially to the Cu surface at the base of pores when porous films are present remains to be investigated.

4. Conclusion

Non-uniform growth of the corrosion products on Cu in aqueous SH^- solutions results in a potential difference between the “thick” and “thin” films. Such a potential difference, though small, leads to variations in corrosion rate since Cu corrosion in aqueous SH^- solutions requires very little overpotential. When this occurs some locations accumulate thick partially protective corrosion films at which the corrosion rate is low while others become covered only with non-protective thin and porous deposits and experience a higher corrosion rate. This leads to the establishment of microgalvanic couples with areas protected by corrosion product deposits acting as cathodes and unprotected areas as anodes.

To sustain these couples Cu transport via surface and/or solution transport processes from anodic locations to cathodic locations must occur. As demonstrated in the geochemical and environmental literature, the Cu transport can be by either soluble Cu(I) complexes or Cu clusters/nanoparticles.

Acknowledgements

This research was funded by the Swedish Nuclear Fuel and Waste Management Co. (SKB, Stockholm, Sweden). The authors

would like to thank Dr. T. Simpson, Dr. C. Wu and Dr. L. Wu for their help with SEM/FIB, ICP-AES and figure preparation, respectively.

References

[1] J.J. De Yoreo, P.G. Vekilov, Principles of crystal nucleation and growth, Rev. Mineral. Geochem. 54 (1) (2003) 57–93.
[2] G.I. Finch, H. Wilman, L. Yang, Crystal growth at the cathode, Discuss. Faraday Soc. 1 (1947) 144–158.
[3] G.H. Nancollas, Kinetics of crystal growth from solution, J. Crys. Growth 3 (1968) 335–339.
[4] P.A. Andrianne, J.P. Dubois, R.F.P. Winand, Electrocrystallization of copper in chloride aqueous solutions, Metall. Trans. B 8 (1) (1977) 315–321.
[5] L.J.W. Shimon, M. Vaida, L. Addadi, M. Lahav, L. Leiserowitz, Molecular recognition at the solid-solution interface: a relay mechanism for the effect of solvent on crystal growth and dissolution, J. Am. Chem. Soc. 112 (17) (1990) 6215–6220.
[6] W.A. Wilcox, Transport phenomena in crystal growth from solution, Prog. Cryst. Growth Charact. Mater. 26 (1993) 153–194.
[7] J. Paquette, R.J. Reeder, Relationship between surface structure, growth mechanism, and trace element incorporation in calcite, Geochim. Cosmochim. Acta 59 (4) (1995) 735–749.
[8] M. Lahav, L. Leiserowitz, The effect of solvent on crystal growth and morphology, Chem. Eng. Sci. 56 (7) (2001), 2245–2225.
[9] J.M. Ouyang, L. Duan, B. Tieke, Effects of carboxylic acids on the crystal growth of calcium oxalate nanoparticles in lecithin-water liposome systems, Langmuir 19 (21) (2003) 8980–8985.
[10] K.K. Caswell, J.N. Wilson, U.H. Bunz, C.J. Murphy, Preferential end-to-end assembly of gold nanorods by biotin-streptavidin connectors, J. Am. Chem. Soc. 125 (46) (2003) 13914–13915.
[11] A.E. Lewis, Review of metal sulphide precipitation, Hydrometallurgy 104 (2) (2010) 222–234.
[12] J. Chen, Z. Qin, D.W. Shoesmith, Kinetics of corrosion film growth on copper in neutral chloride solutions containing small concentrations of sulfide, J. Electrochem. Soc. 157 (2010) C338–C345.
[13] J. Chen, Z. Qin, D.W. Shoesmith, Long-term corrosion of copper in a dilute anaerobic sulfide solution, Electrochim. Acta 56 (2011) 7854–7861.
[14] J. Chen, Z. Qin, D.W. Shoesmith, The rate controlling reactions for copper corrosion in anaerobic aqueous sulphide solutions, Corros. Sci. Eng. Technol. 46 (2011) 138–141.
[15] J. Chen, Z. Qin, D.W. Shoesmith, Copper corrosion in aqueous sulfide solutions under nuclear waste disposal conditions, Mater. Res. Soc. Symp. Proc. 1475 (2012) 465–470.
[16] J. Chen, Z. Qin, L. Wu, J.J. Noël, D.W. Shoesmith, The influence of sulphide transport on the growth and properties of copper sulphide films on copper, Corros. Sci. 87 (2014) 233–238.
[17] J. Chen, Z. Qin, D.W. Shoesmith, Key parameters determining structure and roperties of sulphide films formed on copper corroding in anoxic sulphide solutions, Corros. Eng. Sci. Technol. 49 (2014) 415–419.
[18] D.W. Shoesmith, Assessing the corrosion performance of high-level nuclear waste containers, Corrosion 62 (2006) 703–722.
[19] D. Féron, D. Crusset, J.-M. Gras, Corrosion issues in nuclear waste disposal, J. Nucl. Mater. 378 (2008) 16–23.
[20] F. King, M. Kolar, M. Vahanen, C. Lilja, Modelling long term corrosion behavior of copper canisters in a KBS-3 repository, Corros. Eng. Sci. Technol. 46 (2) (2011) 217–222.
[21] D.D. Wagman, W.H. Evans, V.B. Parker, R.H. Schumm, I. Halow, S.M. Bailey, K.L. Churney, R.L. Nuttall, The NBS tables of chemical thermodynamic properties, J. Phys. Chem. Ref. Data 11 (2) (1982).
[22] J.M. Smith, J.C. Wren, M. Odziemkowski, D.W. Shoesmith, The electrochemical response of preoxidized copper in aqueous sulfide solutions, J. Electrochem. Soc. 154 (8) (2007) C431–C438.
[23] E. Protopopoff, P. Marcus, Potential-pH diagrams for sulfur and hydroxyl adsorbed on copper surfaces in water containing sulfides, sulfites or thiosulfates, Corros. Sci. 45 (2003) 1191–1201.
[24] H.M. Hollmark, P.G. Keech, J.R. Vegelius, L. Werme, L.-C. Duda, X-ray absorption spectroscopy of electrochemically oxidized Cu exposed to Na_2S, Corros. Sci. 54 (2012) 85–89.
[25] E.M. Khairy, N.A. Darwish, Studies on copper-semiconducting layer-electrolyte systems— II. Galvanostatic anodic polarization of $Cu/Cu_2S/S^{2-}$ applying stationary and rectangular pulse techniques, Corros. Sci. 13 (1973) 149–164.
[26] E. Kennard, J.T. Waber, Mathematical study of galvanic corrosion equal coplanar anode and cathode with unequal polarization parameters, J. Electrochem. Soc. 117 (7) (1970) 880–885.
[27] L.A. Shalaby, Galvanic coupling of Ti with Cu and Al alloys in chloride media, Corros. Sci. 11 (10) (1971) 767–778.
[28] F. Mansfeld, E.P. Parry, Galvanic corrosion of bare and coated Al alloys coupled to stainless steel 304 or Ti-6Al-4V, Corros. Sci. 13 (8) (1973) 605–621.
[29] E. Bardal, R. Johnsen, P.O. Gartland, Prediction of galvanic corrosion rates and distribution by means of calculation and experimental models, Corrosion 40 (12) (1984) 628–633.
[30] L.H. Hihara, P.K.M. Kondepudi, The galvanic corrosion of SiC monofilament/ZE41 Mg metal-matrix composite in 0.5 M $NaNO_3$, Corros. Sci. 34 (11) (1993) 1761–1772.
[31] R. Akid, D.J. Mills, A comparison between conventional macroscopic and novel microscopic scanning electrochemical methods to evaluate galvanic corrosion, Corros. Sci. 43 (7) (2001) 1203–1216.
[32] G. Song, B. Johannesson, S. Hapugoda, D. StJohn, Galvanic corrosion of magnesium alloy AZ91D in contact with an aluminium alloy, steel and zinc, Corros. Sci. 46 (4) (2004) 955–977.
[33] E. Tada, S. Satoh, H. Kaneko, The spatial distribution of Zn^{2+} during galvanic corrosion of a Zn/steel couple, Electrochim. Acta 49 (14) (2004) 2279–2285.
[34] R.M. Souto, Y. Gonzalez-Garcia, A.C. Bastos, A.M. Simoes, Investigating corrosion processes in the micrometric range: a SVET study of the galvanic corrosion of zinc coupled with iron, Corros. Sci. 49 (12) (2007) 4568–4580.
[35] K.B. Deshpande, Experimental investigation of galvanic corrosion: comparison between SVET and immersion techniques, Corros. Sci. 52 (2010) 2819–2826.
[36] K.B. Deshpande, Validated numerical modelling of galvanic corrosion for couples: magnesium alloy (AE44)–mild steel and AE44–aluminium alloy (AA6063) in brine solution, Corros. Sci. 52 (10) (2010) 3514–3522.
[37] G.L. Song, Potential and current distributions of one-dimensional galvanic corrosion systems, Corros. Sci. 52 (2) (2010) 455–480.
[38] R.W. Joyner, C.S. McKee, M.W. Roberts, The interaction of hydrogen sulphide with Cu (001), Surf. Sci. 27 (2) (1971) 279–285.
[39] L. Moroney, S. Rassias, M.W. Roberts, Chemisorption of HCl and H_2S by Cu (111)-O surfaces, Surf. Sci. Lett. 105 (1) (1981) L249–L254.
[40] N.P. Prince, D.L. Seymour, M.J. Ashwin, C.F. McConville, D.P. Woodruff, R.G. Jones, A SEXAFS and X-ray standing wave study of the Cu (111)(7×7) R19°-S surface: adsorbate-substrate and adsorbate-adsorbate registry, Surf. Sci. 230 (1) (1990) 13–26.
[41] G.J. Jackson, S.M. Driver, D.P. Woodruff, B.C.C. Cowie, R.G. Jones, The structure of the Cu (111) (7×7) R19°-S surface phase: a new normal-incidence X-ray standing wave study, Surf. Sci. 453 (1) (2000) 183–190.
[42] D.W. Suggs, A.J. Bard, Scanning tunneling microscopic study with atomic resolution of the dissolution of Cu (111) in aqueous chloride solutions, J. Am. Chem. Soc. 116 (1994) 10725–10733.
[43] M.R. Vogt, F.A. Möller, C.M. Schilz, O.M. Magnussen, R.J. Behm, Adsorbate-induced step faceting of Cu (100) electrodes in HCl, Surf. Sci. 367 (1996) L33–L41.
[44] M. Kruft, B. Wohlmann, C. Stuhlmann, K. Wandelt, Chloride adsorption on Cu (111) electrodes in dilute HCl solutions, Surf. Sci. 377 (1997) 601–604.
[45] W.H. Li, R.J. Nichols, An in situ STM study of sulphate adsorption on copper (111) in acidic aqueous electrolytes, J. Electroanal. Chem. 456 (1998) 153–160.
[46] S.E. Bae, K.L. Stewart, A.A. Gewirth, Nitrate adsorption and reduction on Cu (100) in acidic solution, J. Am. Chem. Soc. 129 (2007) 10171–10180.
[47] M.R. Gennero de Chialvo, A.J. Arvia, The electrochemical behaviour of copper in alkaline solutions containing sodium sulphide, J. Appl. Electrochem. 15 (1985) 685–696.
[48] B. Meyer, K. Ward, K. Koshlap, L. Peter, Second dissociation constant of hydrogen sulfide, Inorg. Chem. 22 (1983) 2345–2346.
[49] D. Richard, G.W. Luther III, Chemistry of iron sulfides, Chem. Rev. 107 (2007) 514–562.
[50] D.A. Crerar, H.L. Barnes, Ore solution chemistry V: solubilities of chalcopyrite and chalcocite assemblages in hydrothermal solution at 200 °C and 350 °C, Econ. Geol. 71 (1976) 772–794.
[51] B.W. Mountain, T.M. Steward, The hydrosulphide/sulphide complexes of copper (I): experimental determination of stoichiometry and stability at 22 °C and reassessment of high temperature data, Geochim. Cosmochim. Acta 63 (1999) 11–29.
[52] G.W. Luther III, D.T. Rickard, S. Theberge, A. Olroyd, Determination of metal (bi)sulfide stability constants of Mn^{2+}, Fe^{2+} Co^{2+}, Ni^{2+}, Cu^{2+}, and Zn^{2+} by voltammetric methods, Environ. Sci. Technol. 30 (1996) 671–679.
[53] G.R. Heltz, J.M. Charnock, D.J. Vaughan, C.D. Garner, Multinuclearity of aqueous copper and zinc bisulfide complexes: an EXAFS investigation, Ceochim. Cosmchim. Acta 57 (1993) 15–25.
[54] R.A. Thompson, G.R. Heltz, Copper speciation in sulfide solutions at low sulfur activity: further evidence of cluster complexes, Geochim. Cosmochim. Acta 58 (1994) 2971–2983.
[55] T.F. Rozan, M.E. Lassman, D.P. Ridge, G.W. Luther III, Evidence for iron, copper, zinc complexation as multinuclear sulphide clusters in oxic rivers, Nature 406 (2000) 879–882.